A One-Equation Turbulence Model for Geophysical Applications: Comparison with Data and the k–ε Model

Article *in* Environmental Fluid Mechanics · March 2001

DOI: 10.1023/A:1011560202388

CITATIONS
23

READS
630

2 authors:

Lars B. Axell
Swedish Meteorological and Hydrological Institute
43 PUBLICATIONS **1,583** CITATIONS
SEE PROFILE

Olof Liungman
Bergamotten konsult
16 PUBLICATIONS **350** CITATIONS
SEE PROFILE

A One-Equation Turbulence Model for Geophysical Applications: Comparison with Data and the $k - \varepsilon$ Model

L. B. Axell*
Swedish Meteorological and Hydrological Institute, Norrköping, Sweden

O. Liungman
Department of Oceanography, Earth Sciences Centre, Göteborg University, Göteborg, Sweden

Abstract. A one-equation turbulence model is presented, in which the turbulent kinetic energy k is calculated with a transport equation whereas the turbulent length scale l is calculated with an algebraic expression. The value of l depends on the local stratification and reduces to the classical $\kappa|z|$ scaling for unstratified flows near a wall, where $|z|$ is the distance to the wall. The length scale decreases during stable stratification, and increases for unstable stratification compared to the neutral case. In the limit of strong stable stratification, the so-called buoyancy length scale proportional to $k^{1/2}N^{-1}$ is obtained, where N is the buoyancy frequency. The length scale formulation introduces a single model parameter which is calibrated against experimental data. The model is verified extensively against laboratory measurements and oceanic data, and comparisons are made with the two-equation k-ε model. It is shown that the performance of the proposed k model is almost identical to that of the k-ε model. In addition, the stability functions of Launder are revisited and adjusted to obtain better agreement with recent data.

Keywords: Prandtl number, stability functions, turbulence model, turbulent length scales

1. Introduction

Today there exists a variety of models for calculating turbulent mixing in nature. These range from constant eddy coefficient parameterizations to detailed Large Eddy Simulations and Direct Numerical Simulation [45, 51, 50]. However, due to the computational requirements of the more sophisticated models, geophysical modelers are usually restricted to Turbulent Kinetic Energy (TKE) closure schemes or simpler descriptions. Perhaps the most commonly used turbulence models today are the one-dimensional two-equation models, though sometimes even these, for example in climate modeling, are too computationally expensive.

* Corresponding author. (lars.axell@smhi.se)

Two-equation turbulence models describe turbulence by solving transport equations for the turbulent kinetic energy k and the turbulent macro length scale l, in the k-ε model represented by the dissipation rate ε [46]. Alternatively, the two-equation model of Mellor and Yamada [37] uses transport equations for the turbulence intensity $q^2 = 2k$ and the quantity $2kl$. Note that these two models are very similar despite their different notation [8]. Examples of applications of the Mellor Yamada level 2.5 model on Ocean General Circulation Models can be found in Rosati and Miyakoda [47] and Goose et al. [21]. In the following we will primarily refer to the k-ε model in the context of two-equation models.

Whereas the equation for TKE may be considered well founded in physics, the same is not entirely true for the modeled form of the ε-equation. It is fairly straight-forward to derive the k-equation from the equations of motion under the Boussinesq approximation [28, Chapter 12]. The ε-equation can be derived from the equation of the mean-square vorticity fluctuations, but this requires a scaling argument since the dissipation is not causally related to the vorticity fluctuations [56, Chapter 3.3]. Intuitively it is not obvious that the dissipation should be described by a separate transport equation with a different transport rate from that of k, as is the case in the k-ε model. Furthermore, both the ε-equation and the equation for $2kl$ depend to a greater extent on empirical considerations than the k-equation. For example, there is an ongoing discussion concerning whether the empirical constant multiplying the buoyancy term in the ε-equation should be negative, zero or positive under stable conditions [46, 5, 31]. Recent work has focused on the so-called stability functions that appear as a result of the closure process [15, 26, 5]. These functions, which depend on the stratification and possibly the shear, relate the desired eddy diffusivities to the turbulent quantities k and l, and therefore to a large degree determine the influence of stratification upon turbulent mixing.

Hence, though both the k-ε and the Mellor-Yamada models have proven to work fairly well in many situations, one could argue in favor of replacing the transport equation for the length scale with some other description. Numerous one-equation models have been proposed where the turbulent length scale is determined from an algebraic expression [3, 60, 32]. In general, these are empirical functions of the distance from the nearest boundary, sometimes including modifying functions of k. Other authors have used stratification-related length scales, for example, Gaspar et al. [20], Blanke and Delecluse [4], D'Alessio et al. [11] and Demirov et al. [13].

This paper has two main goals. First, to present a simple yet, in our opinion, physically appealing expression for the turbulent length

scale to be used in one-equation k models. Second, to test the resulting model against laboratory measurements and oceanic data sets, as well as comparing its performance with the more complex two-equation k-ε model. In addition, the stability functions of Launder [30] are revisited and updated using the recent compilation of observational results by Högström [23].

2. Theory

2.1. Hydrodynamic model equations

We will consider the one-dimensional case, that is, we assume horizontal homogeneity in all variables, except for pressure in order to allow for external pressure gradients. This implies that advection may be neglected in all transport equations. Hence, though the model implementation used (see Appendix B) can handle both vertical and horizontal advection (important when modeling, for example, semi-enclosed basins), the vertical advection term will be neglected.

Under these assumptions, the momentum equations are

$$\frac{\partial(\rho u)}{\partial t} = \frac{\partial}{\partial z}\left[\nu_{eff}\frac{\partial(\rho u)}{\partial z}\right] + f\rho v + F_x, \tag{1}$$

$$\frac{\partial(\rho v)}{\partial t} = \frac{\partial}{\partial z}\left[\nu_{eff}\frac{\partial(\rho v)}{\partial z}\right] - f\rho u + F_y, \tag{2}$$

where ρ is the density, u and v are the horizontal velocity components, z is the vertical coordinate (zero at the surface and positive upward), t denotes time, ν_{eff} is the effective viscosity (the sum of the eddy viscosity ν_t and the laminar viscosity ν), f is the Coriolis frequency, and F_x and F_y are source terms such as external pressure gradients. The upper boundary conditions for ρu and ρv are

$$\nu_{eff}\frac{\partial(\rho u)}{\partial z} = \tau_x, \tag{3}$$

$$\nu_{eff}\frac{\partial(\rho v)}{\partial z} = \tau_y, \tag{4}$$

where τ_x and τ_y are the components of the momentum flux at the boundary. This flux is due to wind or ice drift, and may be calculated using standard bulk formulations. At the lower boundary, a zero-velocity condition is used.

The corresponding transport equations for the salinity S and the heat content H are

$$\frac{\partial S}{\partial t} = \frac{\partial}{\partial z}\left(\nu'_{eff}\frac{\partial S}{\partial z}\right) + F_S \tag{5}$$

$$\frac{\partial H}{\partial t} = \frac{\partial}{\partial z}\left(\nu'_{eff}\frac{\partial H}{\partial z}\right) + F_H, \tag{6}$$

where ν'_{eff} is the effective diffusivity (the sum of the eddy diffusivity ν'_t and the respective laminar diffusivities ν_S and ν_H) and F_S and F_H are sources and sinks for salinity and heat respectively. The upper boundary conditions for S and H are

$$\nu'_{eff}\frac{\partial S}{\partial z} = Q_S, \tag{7}$$

$$\nu'_{eff}\frac{\partial H}{\partial z} = Q_H. \tag{8}$$

In (7), Q_S is related to the net freshwater flux due to precipitation and evaporation. Q_H in (8) is the sum of sensible heat flux, latent heat flux, and net long-wave radiation, which are all parameterized using bulk formulae (see sections 4.5 and 4.6 for specifics). The source of heat due to short-wave radiation is handled via the source term F_H, since this will be distributed with depth in the water mass. At the bottom no-flux boundary conditions are used for both heat and salinity.

The temperature T is calculated diagnostically as

$$T = \frac{H}{\rho c_p}, \tag{9}$$

where c_p is the specific heat capacity of water. The density ρ is calculated using a simplified equation of state:

$$\rho = \rho_0[1 - c_{\rho 1}(T - T_r)^2 + c_{\rho 2}S]. \tag{10}$$

Here ρ_0 ($= 10^3$ kg m^{-3}) is a reference density, T_r is the temperature of maximum density, $c_{\rho 1} = 7.18 \times 10^{-6}$ °C^{-2} and $c_{\rho 2} = 8.0 \times 10^{-4}$ psu^{-1}. T_r and $c_{\rho 1}$ have in some cases been adjusted to ensure close agreement with the UNESCO equation of state (see sections 4.5 and 4.6).

2.2. Turbulence closure

To close the set of equations (1)–(10) we require, in addition to expressions for the sources and sinks and appropriate boundary and initial conditions, a way of determining the eddy viscosity ν_t and eddy diffusivity ν'_t. These are estimated from the so-called Kolmogorov-Prandtl relation according to

$$\nu_t = c_\mu k^{1/2} l, \tag{11}$$

$$\nu'_t = c'_\mu k^{1/2} l, \tag{12}$$

where k is the turbulent kinetic energy, l is the turbulent length scale, and c_μ and c'_μ are stability functions (see section 2.2.3). The turbulent kinetic energy k is calculated using the transport equation

$$\frac{\partial k}{\partial t} = \frac{\partial}{\partial z}\left(\frac{\nu_t}{\sigma_k}\frac{\partial k}{\partial z}\right) + P_s + P_b - \varepsilon, \tag{13}$$

where σ_k is the Schmidt number for k and P_s is a source of TKE due to shear given by

$$P_s = \nu_t\left[\left(\frac{\partial u}{\partial z}\right)^2 + \left(\frac{\partial v}{\partial z}\right)^2\right]. \tag{14}$$

The term P_b represents a sink or a source of TKE, depending on whether the stratification is stable or unstable, and is given by

$$P_b = -\nu'_t N^2, \tag{15}$$

where N is the buoyancy frequency defined as

$$N^2 = -\frac{g}{\rho_0}\frac{\partial \rho}{\partial z}$$

and g is the acceleration of gravity. The boundary condition for k is

$$k = \left[\frac{u_*^3}{(c_\mu^0)^3} + \frac{\max(B,0)\kappa d_1}{(c_\mu^0)^3}\right]^{2/3} \tag{16}$$

(see Svensson [53]), where

$$u_* = \left(\frac{\tau}{\rho_0}\right)^{1/2} \tag{17}$$

is the friction velocity at the boundary with τ being the boundary stress, c_μ^0 is a constant equal to the value of c_μ under neutral conditions, and d_1 is the distance from the boundary to the center of the near-boundary grid cell. B is the buoyancy flux at the boundary (positive upward), given by

$$B = -\frac{g}{\rho_0}\left(\frac{\partial \rho}{\partial T}\frac{Q_H}{\rho_0 c_p} + \frac{\partial \rho}{\partial S}Q_S\right). \tag{18}$$

Thus, only a destabilizing buoyancy flux affects the boundary condition on k, which is consistent with the concept of intensified turbulence due to convection.

To complete the closure either ε or l must be determined, and by dimensional arguments these are related by

$$l = (c_\mu^0)^3 \frac{k^{3/2}}{\varepsilon}. \tag{19}$$

The proportionality constant in (19) is required to be $(c_\mu^0)^3$ if the logarithmic law is to be fulfilled in a non-buoyant constant-stress boundary layer; see for example Burchard et al. [8].

2.2.1. *The k-ε model*

In the k-ε model the dissipation rate ε is determined from the transport equation

$$\frac{\partial \varepsilon}{\partial t} = \frac{\partial}{\partial z}\left(\frac{\nu_t}{\sigma_\varepsilon}\frac{\partial \varepsilon}{\partial z}\right) + \frac{\varepsilon}{k}\left(c_{\varepsilon 1} P_s + c_{\varepsilon 3} P_b - c_{\varepsilon 2}\varepsilon\right), \tag{20}$$

where σ_ε is the Schmidt number for ε, and $c_{\varepsilon 1}$, $c_{\varepsilon 2}$, and $c_{\varepsilon 3}$ are empirical constants in the model; see Table I. The boundary condition for ε is

$$\varepsilon = \left(c_\mu^0\right)^3 \frac{k^{3/2}}{\kappa d_1}.$$

Several authors [15, 32, 8] have applied stratification-dependent lower limits on ε or, equivalently, a lower bound on l, to simulate the limiting effect of stable stratification on the size of the turbulent eddies. These take the form

$$\varepsilon \geq CkN. \tag{21}$$

The suggested value for C is about 0.22. For further details on the k-ε model, see for example Rodi [46] or Burchard and Baumert [5].

2.2.2. *The k model*

In the k model, closure is achieved by calculating the turbulent length scale l from an algebraic expression, rather than solving an additional transport equation. The dissipation rate ε is then determined using (19). In this section we will argue in favor of a simple and physically intuitive expression for the turbulent length scale l, by making the assumption that l is determined locally at each instant. In other words, we will assume that l is only indirectly affected by transport of turbulent quantities and does not have a memory of earlier events other than through k.

Perhaps the most thoroughly investigated turbulent flows are wall-bounded, neutral shear flows, where theoretical and experimental results have shown the validity of the logarithmic law [56]. Near a wall the turbulence will be influenced by the distance to the wall d, in our

Table I. Numerical values of the constants in the turbulence models.

Constant	k-ε model	k model
c_μ^0	0.5562	0.5562
σ_k	1.0	1.0
σ_ε	1.08	–
$c_{\varepsilon 1}$	1.44	–
$c_{\varepsilon 2}$	1.92	–
$c_{\varepsilon 3}$ $(N^2 > 0)$	-1.1	–
$c_{\varepsilon 3}$ $(N^2 < 0)$	1.0	–
c_b	–	0.35

case the distance to the surface or bottom. An appropriate estimate for the turbulent length scale is κd, where κ is von Karman's constant $(= 0.40)$, and for a rough surface we hence define the geometric length scale

$$l_g = \kappa\,(d + z_0)\,, \tag{22}$$

which is the turbulent length scale in the limit of neutral shear flow near a wall. Here, z_0 is the roughness parameter of the wall.

Two fundamental frequencies of a geophysical flow are the buoyancy frequency N and the Coriolis frequency f. Based on these frequencies we can define length scales using the velocity scale of the turbulent motions $k^{1/2}$. However, rotational effects on the turbulent motions will be neglected as these can be assumed to be small in geophysical applications [16]. Hence, we are left with a buoyancy length scale l_b, here defined as

$$l_b = c_b \frac{k^{1/2}}{N}, \tag{23}$$

which is the turbulent length scale in the limit of strong, stable stratification away from walls, with c_b a constant of proportionality. Note that l_b is undefined for unstable stratification $(N^2 < 0)$. This limiting length scale was already introduced by Galperin et al. [15] in the Mellor-Yamada hierarchy of turbulence models.

The hypothesis is that the turbulent length scale is a function of the geometric and buoyancy length scales. In the case of stable stratification, a first choice would perhaps be that l should equal the smallest of l_g and l_b, that is $l = \min(l_g, l_b)$. However, it is not impossible that both the proximity of a wall and the local stratification could influence

l simultaneously. One could then envisage an algebraic formula such as

$$\frac{1}{l^n} = \frac{1}{l_g^n} + \frac{1}{l_b^n}. \tag{24}$$

Note that $n \to \infty$ yields the minimum formula, and that $n = 1$ yields the well-known Blackadar formula

$$l = \frac{\kappa (d + z_0)}{1 + \kappa d / l_0} = \frac{l_g l_0}{l_g + l_0} \tag{25}$$

if $l_0 = l_b$ [3, 11]. However, we choose $n = 2$, as this will allow us to generalize (24) to be valid in unstable situations. Thus, we have

$$\frac{1}{l^2} = \frac{1}{l_g^2} + \frac{N^2}{c_b^2 k}. \tag{26}$$

The expression (26) has the following desirable properties. In a neutral mixed layer near a boundary ($N^2 = 0$), l reduces to the expected "law-of-the-wall" behavior given by (22). The physical interpretation is that the size of the most energetic turbulent eddies is limited by the distance to the nearest boundary. In the case of two boundaries, for example bottom and surface, we can write

$$\frac{1}{l_g^2} = \frac{1}{\kappa^2 (-z + z_0)^2} + \frac{1}{\kappa^2 (D + z + z_0)^2}$$

instead of (22), where D is the total depth. This yields the commonly used parabolic profile for l in a neutral environment [37, 8].

In a stable environment ($N^2 > 0$) l is reduced compared to the non-buoyant flow. In the case of a strong, stable stratification sufficiently far away from the boundaries $l \to l_b$ (cf. Galperin et al. [15]). The physical interpretation of l_b is that the size of the most energetic eddies is limited by the stratification, since they have to perform work against gravity. According to the relation (19) this limit is equivalent to the lower limit on ε [Eq. (21)] if $C = \left(c_\mu^0\right)^3 c_b^{-1}$, and hence there is no need to limit ε in the k model.

In a locally unstable environment ($N^2 < 0$), l becomes larger than in the neutral case. This is consistent with the data of McPhee [34], who showed that during unstable conditions the so-called mixing length, defined as the eddy viscosity divided by the square root of the local kinematic stress, increased away from the surface at a higher rate than predicted by κd scaling. Note that Eq. (26) will fail in the case of strong convection, if $N^2 \leq -c_b^2 k l_g^{-2}$. To avoid this problem, let us rewrite (26)

in a form more suitable for convection. Multiplying (26) by $l^2 l_g^2$ yields

$$l^2 = l_g^2 - \frac{l^2 l_g^2 N^2}{c_b^2 k}, \tag{27}$$

and if we substitute (19) for l only on the right-hand side of (27), we obtain

$$l^2 = l_g^2 \left[1 - \frac{(c_\mu^0)^6 k^2 N^2}{\varepsilon^2 c_b^2} \right],$$

or

$$l = l_g \left[1 - (c_\mu^0)^6 c_b^{-2} R_t \right]^{1/2}, \tag{28}$$

where we have introduced the turbulent Richardson number

$$R_t = \frac{k^2 N^2}{\varepsilon^2}. \tag{29}$$

Hence, using (28) in the case of unstable stratification ($R_t < 0$), $l > l_g$ and is always finite and real. Note, however, that (28) will yield an imaginary l during very stable conditions, if $R_t > c_b^2 (c_\mu^0)^{-6}$. For moderate stratification, stable or unstable, (26) and (28) are equivalent. To conclude, Eq. (26) will be used if $N^2 \geq 0$ and Eq. (28) when $N^2 < 0$.

2.2.3. *Stability functions*

The stability functions c_μ and c'_μ introduced above include further corrections for the effect of stratification on the transport of Reynolds stresses and fluxes of heat and salt. The turbulent Prandtl number σ_t is defined as the ratio between eddy viscosity ν_t and eddy diffusivity ν'_t or, equivalently, the ratio between c_μ and c'_μ, that is

$$\sigma_t = \frac{\nu_t}{\nu'_t} = \frac{c_\mu}{c'_\mu} \tag{30}$$

[cf. (11)–(12) above].

The stability functions of Launder [30] imply a turbulent Prandtl number in the range $0.6 < \sigma_t < 2.0$ for stable stratification. He estimated the coefficients of his stability functions from the laboratory data of Webster [58] and Champagne et al. [10]. However, it is sometimes difficult to obtain Reynolds numbers in the laboratory as high as in the ocean or the atmosphere and the proximity of lateral boundaries in the laboratory may affect the results. Also, Webster [58] feared that his experiment was not in total equilibrium. This indicates that the numerical values of the coefficients reported by Launder [30] may be somewhat uncertain. Further, the corresponding range of Prandtl number for the stability functions of Galperin et al. [15], Kantha and

Clayson [26], and Luyten et al. [32] are $0.8 < \sigma_t < 0.9$, $0.7 < \sigma_t < 1.2$, and $0.7 < \sigma_t < 1.5$, respectively. These sets of stability functions seem to have been calibrated using data from the famous Kansas experiment reported by Businger et al. [9]. However, these data have been shown to suffer from flow distortion [59]. An indication of this is that the derived value of von Karman's constant from these data was 0.35, which is outside the normally accepted range $0.39 < \kappa < 0.41$. Högström [23] investigated a much larger data set, including data from the Kansas experiment, and corrected for flow distortion when necessary. He found turbulent Prandtl numbers in the range $1.0 < \sigma_t < 1.4$ for $0.0 < \zeta < 0.5$ (i.e., neutral to stable stratification), where ζ is the distance from the boundary normalized with the Monin-Obukhov length. Because none of the above-mentioned stability functions agree with the results of Högström, we choose to tune the stability functions of Launder [30]. The details of the reevaluation of the coefficients in the stability functions can be found in Appendix A.

The resulting stability functions are

$$\begin{aligned} c_\mu &= \frac{c_\mu^0[\phi/\phi_T + (c_T'/\phi_T - 1)\phi\phi_T' R_t]}{[1 + (\phi_T' c_T' + 2\phi\phi_T)R_t](1 + \phi\phi_T R_t)} \\ &\approx \frac{0.556 + 0.108R_t}{1 + 0.308R_t + 0.00837R_t^2}, \end{aligned} \tag{31}$$

$$\begin{aligned} c_\mu' &= \frac{c_\mu^0}{1 + (\phi_T' c_T' + 2\phi\phi_T)R_t} \\ &\approx \frac{0.556}{1 + 0.277R_t}, \end{aligned} \tag{32}$$

which corresponds to a turbulent Prandtl number σ_t given by

$$\begin{aligned} \sigma_t &= \frac{\phi/\phi_T + (c_T'/\phi_T - 1)\phi\phi_T' R_t}{1 + \phi\phi_T R_t} \\ &\approx \frac{1 + 0.193R_t}{1 + 0.0302R_t}. \end{aligned} \tag{33}$$

All numerical values are listed in Table II, along with the estimates proposed by Launder.

It should be mentioned that as $R_t \to +\infty$, $c_\mu' \to 0$ according to (32) and the flux Richardson number $R_f \to R_f^c \approx 0.257$ [see Eq. (A12) in Appendix A]. This agrees well with reported values of R_f^c, the critical flux Richardson number, which usually are in the range $0.15 < R_f^c < 0.32$ [57, 37, 40, 38, 5].

Table II. Values of coefficients in the stability functions.

Coefficient	Launder [30]	Present authors
ϕ	0.20	0.174
ϕ_T	0.31	0.174
ϕ'_T	0.13	0.136
c'_T	1.6	1.6

For c'_μ to be finite and positive during strong convection Eqs. (31) and (33) require that $R_t > -5.1$. Similarly, (32) demands that $R_t > -3.6$. However, a too sharp cut-off of the stability functions at these values for R_t may introduce numerical instabilities. Exactly the same problem occurs for the stability functions of Galperin et al. [15]. We will adopt the solution proposed by Burchard and Petersen [7], who introduced a smoothing function for R_t to ensure a gentle transition into the regime of strong convection. In the present notation the smoothing function of Burchard and Petersen [7] becomes

$$\widetilde{R}_t = \max\left[R_t, R_t - \frac{(R_t - R_t^c)^2}{R_t + R_t^{min} - 2R_t^c}\right],$$

where $\widetilde{R}_t$ replaces R_t in (31)–(33) when $R_t < R_t^c$. Numerical experiments indicate that $R_t^c = -1.0$ and $R_t^{min} = -3.0$ are suitable values. The resulting stability functions and Prandtl number are shown in Figure 1 as functions of R_t, R_f and the gradient Richardson number $R_g = \sigma_t R_f$.

3. Model calibration

Before evaluating the performance of the proposed model we must determine the numerical value of the coefficient c_b in (23). This was done by simulating a Kato-Phillips type experiment, that is the deepening of a mixed layer in a stably stratified fluid due to surface stress, and matching the results to the solution of Price [44]. Based on the results of Kato and Phillips [27], Price determined that the mixed layer depth D_{ml} should vary with time t according to

$$D_{ml}(t) = 1.05 u_* N_0^{-1/2} t^{1/2},$$

where N_0 is the constant initial buoyancy frequency. To make comparison easier, we have used the same values for N_0 and u_* as Burchard

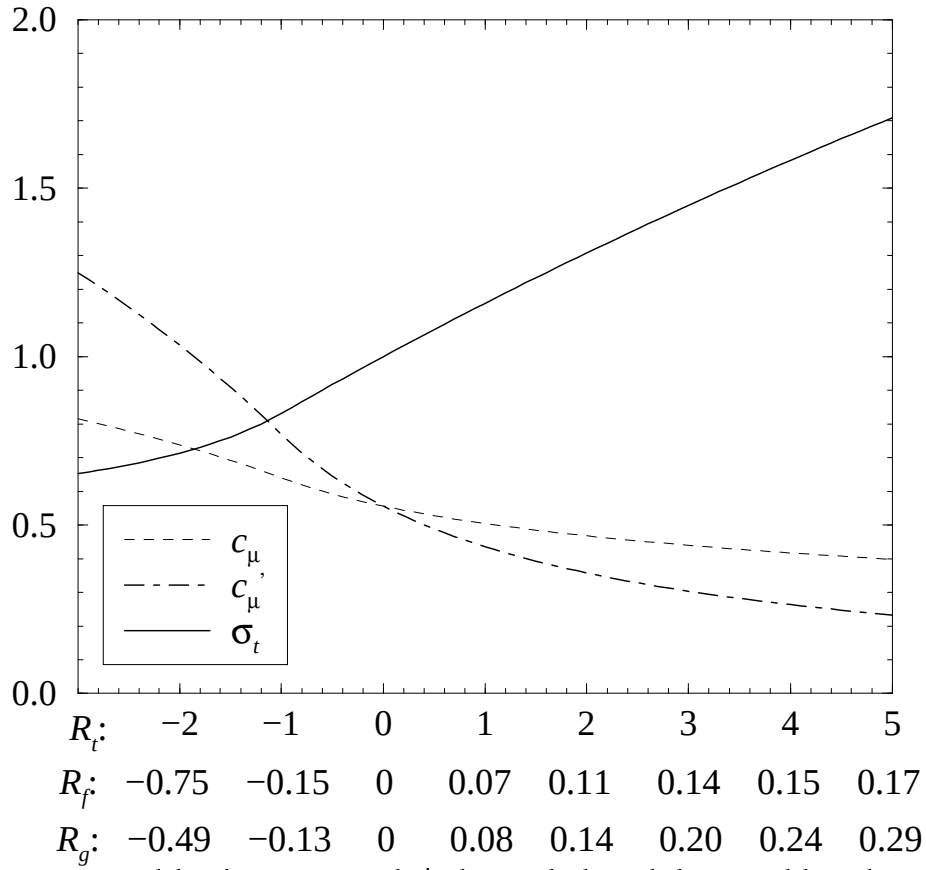

Figure 1. Stability functions c_μ and c'_μ along with the turbulent Prandtl number $\sigma_t = c_\mu / c'_\mu$.

et al. [8], namely 10^{-2} s^{-1} and 10^{-2} m s^{-1} respectively, as well as the same temporal and vertical resolution ($\Delta t = 30$ s, $\Delta z = 0.25$ m). To determine D_{ml} from the computed stratification, both a maximum density gradient and a TKE extinction criterion were used (viz. $k < 10^{-6}$ m^2 s^{-2}; see for example D'Alessio et al. [11]), but the difference proved negligible. The constant c_b was adjusted in small steps until the best fit with the empirical curve was achieved. The results for $c_b = 0.35$ are shown in Fig. 2. The agreement was not very sensitive to the exact value of c_b, that is, a 10% change still yielded results on par with those presented by other authors (cf. Fig. 4 in Burchard et al. [8]). We conclude that $c_b = 0.35$ is a suitable value. Note that the value of c_b depends on the choice of stability functions. With constant stability functions, that is $c_\mu = c'_\mu = c^0_\mu$, best fit was achieved with $c_b = 0.30$.

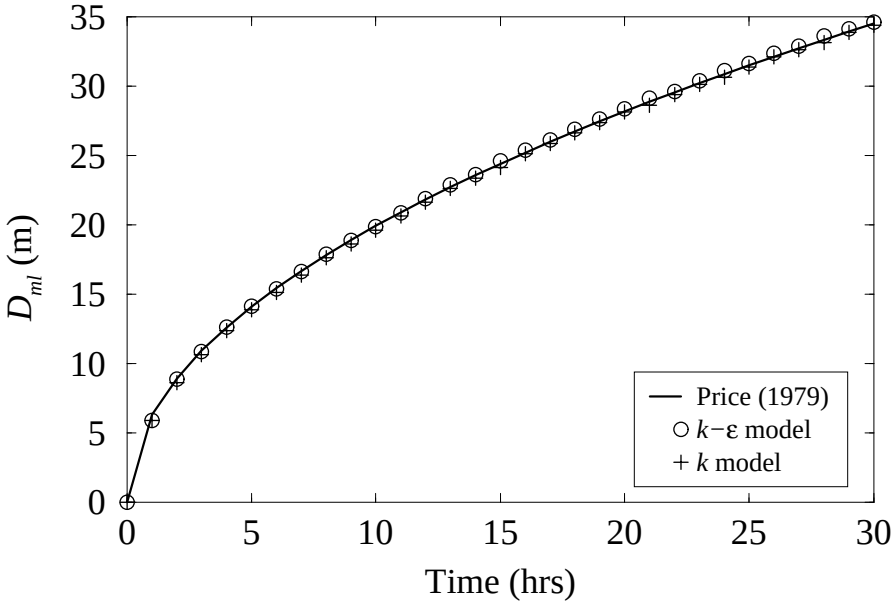

Figure 2. Simulated mixed layer deepening compared to the algebraic formula of Price [44].

Since the value of the coefficient $c_{\varepsilon 3}$ in the k-ε model [see Eq. (20)] also depends on the formulation of the stability functions, the same calibration was performed for this coefficient. The result was $c_{\varepsilon 3} = -1.1$ for stable stratification (see Table I and Fig. 2). For the case of unstable stratification we adopt the value used by Burchard et al. [8], that is $c_{\varepsilon 3} = +1.0$.

In Fig. 3 the profiles of k, l and ν_t after 30 hours are shown for the k and the k-ε models. It is clear that the k model produces profiles very similar to those of the k-ε model.

4. Model verification

4.1. The logarithmic law

As a first test we will confirm that the proposed k model fulfills the logarithmic law near a wall boundary in a non-buoyant shear flow. To this end, let us consider the model equations in the case of steady state, no rotation, no external pressure gradients, no stratification, and no influence from the farther boundary (infinitely deep fluid). Then the

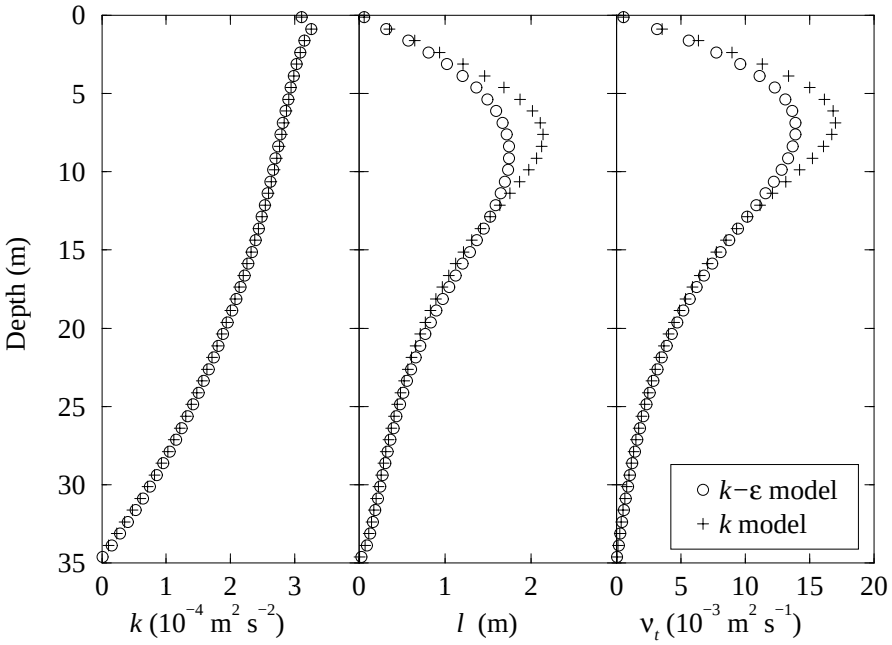

Figure 3. Vertical profiles of k (left), l (middle), and ν_t (right) from the Kato-Phillips type entrainment experiment.

x-momentum equation (1) reduces to

$$\frac{\partial}{\partial z}\left[\nu_{eff}\frac{\partial(\rho u)}{\partial z}\right] = 0. \tag{34}$$

If we integrate (34) from the boundary at $z = 0$ to some level near the boundary, neglect molecular viscosity and assume that there exists a constant-stress layer close to the boundary, then we have to a good approximation

$$\nu_t u_z = u_*^2, \tag{35}$$

where we have used (17), and $u_z = \partial u/\partial z$.

Using the same assumptions as above and additionally assume that k is approximately constant in this layer, the TKE equation (13) reduces to

$$\nu_t u_z^2 = (c_\mu^0)^3 \frac{k^{3/2}}{\kappa|z + z_0|}, \tag{36}$$

where (19) has been used and it has been recognized that $l = \kappa|z + z_0|$. From the boundary condition (16) we have

$$k = \frac{u_*^2}{(c_\mu)^2}, \tag{37}$$

which inserted into (36) yields

$$\nu_t u_z^2 = \frac{u_*^3}{\kappa|z+z_0|}. \tag{38}$$

Now, eliminating ν_t between (35) and (38) yields

$$u_z = \frac{u_*}{\kappa|z+z_0|},$$

which after integration can be written

$$\frac{u}{u_*} = \kappa^{-1} \ln\left|\frac{z+z_0}{z_0}\right|. \tag{39}$$

Similarly, we can solve for the eddy viscosity between (35) and (38), which results in

$$\nu_t = u_* \kappa (z+z_0). \tag{40}$$

Equations (39) and (40) are the well-known theoretical results of the logarithmic layer, that is, a logarithmic velocity distribution and a linear profile of the eddy viscosity cited in for example Kundu [28, Chapter 12].

4.2. Monin-Obukhov similarity

In a flow near a boundary, typically corresponding to the lower tens of meters in the atmosphere, the dynamics is controlled by the boundary fluxes of momentum and buoyancy. Let us introduce a non-dimensional distance ζ from the nearest boundary,

$$\zeta = \frac{z+z_0}{L_{MO}}, \tag{41}$$

where the so-called Monin-Obukhov length L_{MO} is defined as

$$L_{MO} = -\frac{u_*^3}{\kappa B}. \tag{42}$$

The von Karman constant κ is included for convenience, and B is the buoyancy flux at the boundary (positive upward) given by (18). For stable situations $\zeta > 0$, and for unstable situations $\zeta < 0$. In the region where $-1 < \zeta < 0$ we have what is called forced convection, that is, the shear production of TKE is larger than the buoyancy production. Conversely, the region $\zeta \ll -1$, where the buoyancy production of TKE dominates over shear production, is a region of free convection [28].

The empirical Monin-Obukhov similarity relations relate the gradients of velocity u and (potential) temperature T to ζ according to

$$\frac{\partial u}{\partial z} = \frac{u_*}{\kappa|z+z_0|}\Phi_m(\zeta), \tag{43}$$

$$\frac{\partial T}{\partial z} = \frac{\theta_*}{\kappa|z+z_0|}\Phi_h(\zeta), \tag{44}$$

where $\theta_* = -\overline{w'T'}/u_*$ is the friction temperature, in analogy with the friction velocity, and $\overline{w'T'}$ is the vertical, turbulent heat transport. It is easy to show that

$$\sigma_t = \frac{\Phi_h}{\Phi_m}. \tag{45}$$

Based on a large amount of observations reported by different authors, Högström [23] determined the following empirical relationships:

$$\Phi_m(\zeta) = \begin{cases} 1+5.3\zeta & ;\ 0 \le \zeta \le 0.5 \\ (1-19\zeta)^{-1/4} & ;\ -2.0 \le \zeta < 0 \end{cases} \tag{46}$$

$$\Phi_h(\zeta) = \begin{cases} 1+8.0\zeta & ;\ 0 \le \zeta \le 0.5 \\ 0.95(1-11.6\zeta)^{-1/2} & ;\ -2.0 \le \zeta < 0 \end{cases} \tag{47}$$

In this section we will show how well the proposed k model and the proposed stability functions can simulate the so-called Monin-Obukhov similarity relations, by looking for an analytical solution to the model equations in the case of relatively small deviations from the neutral case. To accomplish this we make the following assumptions: 1) steady state, 2) negligible turbulent transport of k, 3) infinitely deep fluid, and 4) constant momentum flux near the boundary.

Under these conditions the TKE equation (13) may be written

$$P_s(1-R_f) = \varepsilon, \tag{48}$$

where (A9) has been used. Further, using (11), (14) and (19) we see that (48) can be expressed as

$$c_\mu k^{1/2} l u_z^2 (1-R_f) = \frac{(c_\mu^0)^3 k^{3/2}}{l}. \tag{49}$$

It is easy to show that the boundary condition (16) can be written

$$k = \frac{(1-R_f)^{2/3} u_*^2}{(c_\mu^0)^2}$$

[cf. (37)], which inserted into (49) yields

$$\left(\frac{u_z l}{u_*}\right)^2 = \frac{c_\mu^0}{c_\mu (1 - R_f)^{1/3}}. \tag{50}$$

Now, if we substitute (28) (which is valid for $-\infty < R_t < +4.1$, or about $-\infty < \zeta < +1.1$) into (50) and use (43), we finally get

$$\Phi_m = \sqrt{\frac{c_\mu^0}{c_\mu [1 - R_f]^{1/3} [1 - (c_\mu^0)^6 c_b^{-2} R_t]}}. \tag{51}$$

Then, from (30) and (45) we see that $\Phi_h = \Phi_m c_\mu / c'_\mu$, which yields

$$\Phi_h = \sqrt{\frac{c_\mu^0 c_\mu}{c_\mu'^2 [1 - R_f]^{1/3} [1 - (c_\mu^0)^6 c_b^{-2} R_t]}}. \tag{52}$$

In (51) and (52), c_μ^0 and c_b are constants and c_μ and c'_μ are given by (31) and (32), respectively. R_t and R_f are related according to (A12), but to compare the result with the empirical relations (46) and (47) we need a relation between ζ and R_t or R_f. From (18), (41) and (42) we have

$$\zeta = \frac{\kappa |z + z_0| g (\partial \rho / \partial T) \overline{w'T'}}{\rho_0 u_*^3}, \tag{53}$$

where $\overline{w'T'} = Q_h / (\rho_0 c_p)$ is the heat flux at the boundary, and we have set $Q_s = 0$. Further, the flux Richardson number can be written

$$R_f = -\frac{P_b}{P_s} = \frac{\nu'_t N^2}{\nu_t u_z^2} = \frac{g (\partial \rho / \partial T) \overline{w'T'}}{\rho_0 \nu_t u_z^2}. \tag{54}$$

If we finally assume a constant-stress layer near the boundary, we can use (35) in (54) to obtain

$$R_f = \frac{g (\partial \rho / \partial T) \overline{w'T'}}{\rho_0 u_*^2 u_z}. \tag{55}$$

Finally, substituting (43) and (55) into (53) yields

$$\zeta = \Phi_m R_f. \tag{56}$$

If we set $R_f = 0$ and $R_t = 0$, then (51), (52) and (56) form the solution hinted at by Mellor and Yamada [36] in the limit of only weak stratification.

Figure 4 shows the result compared with the empirical relations Φ_m, Φ_h, and $\sigma_t = \Phi_h / \Phi_m$. Clearly, the k model in combination with

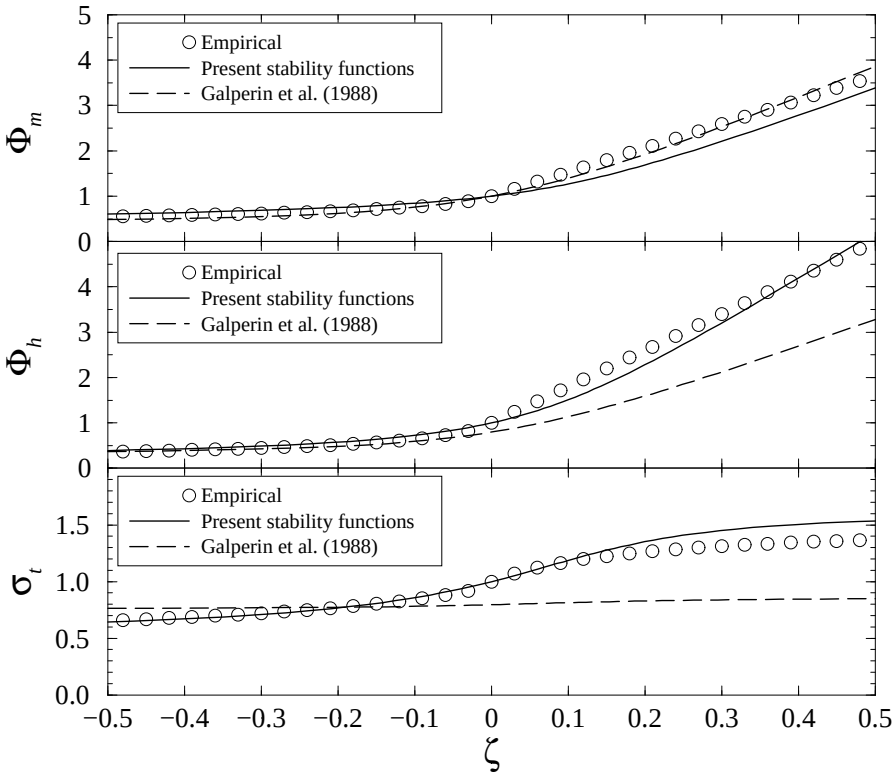

Figure 4. Comparison between the empirical Monin-Obukhov similarity functions Φ_m (upper panel) and Φ_h (middle panel) of Högström [23], and those calculated from the analytical k model equations. Also shown is the corresponding turbulent Prandtl number $\sigma_t = \Phi_h/\Phi_m$ (lower panel). For comparison, the corresponding result with the widely used stability functions of Galperin et al. [15] are also included. ζ is the distance from the boundary scaled by the Monin-Obukhov length.

the proposed stability functions agrees fairly well with the empirical data, but during stable conditions ($\zeta > 0$) the velocity gradient (Φ_m) is somewhat underestimated. Also shown is the corresponding analytical result with the k model, but with the widely used stability functions of Galperin et al. [15]. These stability functions clearly yield poorer agreement with the recent empirical data of Högström [23].

That the assumptions leading to (51), (52) and (56) are fair is supported by results from numerical simulations with the full k model (not shown), which produced almost identical results. In addition, using the same stability functions with the k-ε model yielded very similar results.

4.3. Simulation of idealized entrainment experiments

Next the k model was tested by calculating the mixed-layer depth in some of the idealized numerical experiments of Martin [33] and D'Alessio et al. [11]. The purpose is to show how the k model performs in relation to other well-known mixed-layer models. Here, the mixed-layer depth is defined as the depth of the upper boundary of the most shallow computational cell in which the TKE first falls below 10^{-6} m^2 s^{-2} (TKE extinction criterion). Various numerical experiments were conducted, with different heat and momentum fluxes through the sea surface. In all experiments the inertial period was 24 hours. The salinity fields were constant at 35 psu and all simulations were started from a state of rest. For comparison, all experiments were conducted with both the k-ε and the k models.

In the first experiment the surface heat flux was zero. The initial stratification was stable with a sea-surface temperature of 24°C and a linear decrease of 0.05°C m^{-1}. The model was forced for five days with a constant wind stress of 0.1 N m^{-2}.

In the second experiment the ocean was heated from above by a constant heat flux of 600 ly day^{-1} (= 290 W m^{-2}). The initial temperature was constant at 19°C down to 100 m depth, and then decreased linearly by 0.05°C m^{-1} down to the bottom. The model was forced for two days with the same constant wind stress as in the previous experiment.

The third experiment was initialized as the first experiment, but the ocean was cooled at the surface by a constant heat flux of 200 ly day^{-1} (= 97 W m^{-2}) for a period of 120 days (corresponding to a winter season). Again, the wind stress was constant at 0.1 N m^{-2}.

The fourth experiment simulated free convection, with a constant cooling rate at the surface of 100 W m^{-2} and no wind stress. Initially the sea-surface temperature was 22°C and the stratification was stable with a gradient of 0.1°C m^{-1}. In this experiment the model was forced for three days.

Table III shows the final mixed-layer depths from the four experiments, including corresponding results for the Mellor-Yamada level 2.5 model [33] and the model of D'Alessio et al. [11]. The performance of the k and k-ε models is very similar. The k model appears to produce a deeper mixed-layer depth in the cooling case, whereas the k-ε model mixes slightly deeper when there is no buoyancy forcing. For both models the results are similar to those obtained using the other two mixed-layer models, though at the low end of the range in the case with surface heating. It should be emphasized that the chosen stability functions (31) and (32) reduce the eddy diffusivities for salinity and

Table III. Calculated mixed-layer depths (in meters) in entrainment experiments with idealized forcing.

	No heat flux	Heating	Cooling	Free convection
k model	20	14	113.5	13
k-ε model	21.5	14.5	108	13
Mellor-Yamada 2.5	18	14	103	–
D'Alessio et al. [11]	23	19	109	12.8

temperature during stable stratification more than those of, for example, Galperin et al. [15]. This is because the stability functions used in the present study yield a modeled Φ_h which agrees with the empirical formulae proposed by Högström [23]. For positive ζ, Högström's expression indicates larger gradients (less mixing) than other common formulae for Φ_h [9, 29].

4.4. Simulation of free convection in the laboratory

Though the closure assumptions made when deriving one- and two-equation TKE models do not take into account the large-scale, partly ordered motions of convection, any turbulence model must behave reasonably in the case of convection if it is to be at all useful in geophysical applications. A popular test of a model's ability to simulate free convection are the laboratory experiments of Deardorff et al. [12] (see, for example, Svensson [53] and Burchard and Petersen [7]). In these, a cylindrical vessel of thermally stratified water was heated from below while continuously measuring the temperature profiles. In experiment A of Deardorff et al. [12], the initial bottom temperature and temperature gradient were 21.5 °C and 45 °C m^{-1}, respectively. In the model simulations, forcing at the bottom boundary is provided by the measured heat fluxes for $z = 0$ presented by Deardorff et al. in their Fig. 7. We have assumed the same heat flux at $t = 0$ and $t = 1$ minute, and used linear interpolation for times between those for which data are available. The average heat flux was approximately 12.5×10^3 W m^{-2}. See Table B1 for further details.

The simulation was run for both the k and the k-ε models, and the results are shown in Fig. 5. Both models show reasonable agreement with data. The most obvious difference is that the simulations produce unstable or neutral stratification in the convecting layer, due to the down-gradient transport assumption, whereas in the measurements the

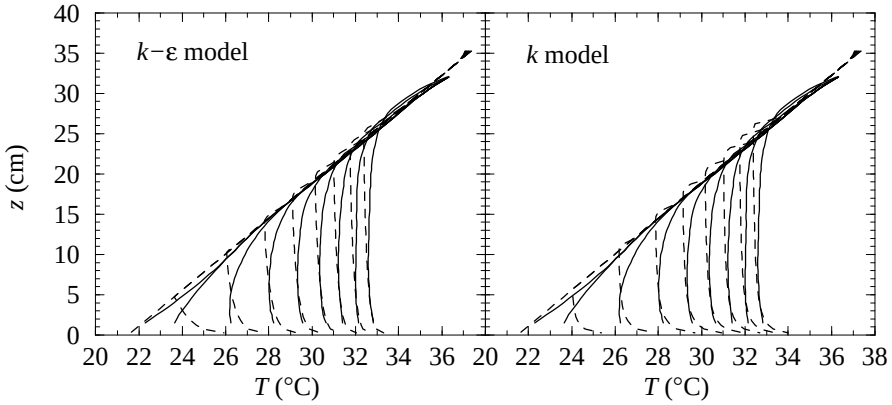

Figure 5. Measured (solid) and simulated (dashed) temperature profiles by the k-ε (left) and k (right) models at $t = 0$, 27, 83, 144, 203, 263, 322, 383 and 440 s after the beginning of experiment A. Data from Fig. 4 in Deardorff et al. [12].

stratification is mostly stable or neutral. (Note that the pronounced counter-gradient slopes of the measured profiles at $t = 27$ and 83 s may be disregarded, as they are a result of time averaging during the early, rapid rise of the interface between convecting and quiescent fluid [12].) However, near the bottom, below the lowest level of measurement, Deardorff et al. report that the observed temperature profiles also exhibited a strong, negative gradient.

The performance of the k model is almost identical to that of the k-ε model. The former appears to respond quicker and produces somewhat stronger mixing (weaker temperature gradient) at earlier times, but overestimates the interface height somewhat.

4.5. Simulation of dissipation in the Irish Sea

In this verification test we will attempt to reproduce the dissipation measurements in the Irish Sea presented by Simpson et al. [49]. We will consider the observations from the stratified site S1 (53°49′ N, 5°27′ W), with a total depth of 90 m. Profiles of turbulent dissipation, conductivity and temperature, as well as current velocities at fixed depths, were measured regularly over a 24-hour period in July, 1993. Site S1 is dominated by rectilinear tidal currents and is stratified in respect to both temperature and salinity. This data set was also used by Burchard et al. [8] when comparing the k-ε and the Mellor-Yamada models.

The barotropic pressure forcing due to the tides was calculated from observed current velocities by solving the momentum equations (1) and (2) as follows. The diffusion of momentum was taken as that calculated

by the model during the previous time step. The time derivative was approximated as the difference between the current measured by the deepest moored current meter (8 m above the bottom) and the current calculated by the model at the same level during the previous time step, divided by the length of the time step. The resultant source terms $F_{x,y}$ were then assumed to represent the barotropic pressure gradients due to the tides for the following time step. This method constitutes a relaxation of the modeled current towards the observed current at the level of the deepest moored current meter [8].

In contrast to Burchard et al. [8] and Simpson et al. [49], we do not neglect horizontal advection as observations clearly indicate that this dominates the variability in the salinity and temperature stratification [see, for example, Fig. 6a in Simpson et al.]. Hence, we included a constant advective horizontal flow in each computational cell, where inflowing water had properties equal to those observed at that time and outflowing water had properties equal to modeled values. This mimics the advective transport of salinity and heat through the model area, and provides a relaxation towards the observed stratification such that the simulated stratification agrees well with that observed (not shown).

The model was also forced by surface stress calculated from observed wind speed and direction, as well as the heat flux through the surface determined from observed dew point temperature and irradiance according to Simpson and Bowers [48]. Measured temperature and salinity profiles supply the initial conditions. The model was spun up for one hour with the stratification fixed at the initial values. The constants in the simplified equation of state (10) were adjusted as follows: $c_{\rho 1} = 6.3 \times 10^{-6}$ °C^{-2} and $T_r = 3.98 - 0.2\overline{S}$ °C, where $\overline{S}$ is the mean salinity (see Table B1 for other numerical parameters).

Figure 6 shows isopleths of observed and simulated dissipation. The qualitative agreement between observations and model results is good. Both the k-ε and the k model clearly capture the tidal fluctuations of the dissipation in the bottom boundary layer. The magnitudes are also reasonable, though details may differ. Away from the boundaries, in the weakly stratified interior (approximately between 15 and 55 m depth), the modeled dissipation levels are a result of tuning the minimum value for the TKE, k_{min} (see section 5). Otherwise both models, as well as the Mellor-Yamada model [49, 8], fail to reproduce the observed dissipation levels in the interior. In the results presented here $k_{min} = 4 \times 10^{-6}$ m^2 s^{-2}. The small variations of the modeled dissipation in the interior are caused by changes in the stratification due to advection.

The mean dissipation profiles show that the two models also agree well quantitatively with observations (Fig. 7). However, for the k-ε model to produce the same agreement with observations in the bottom

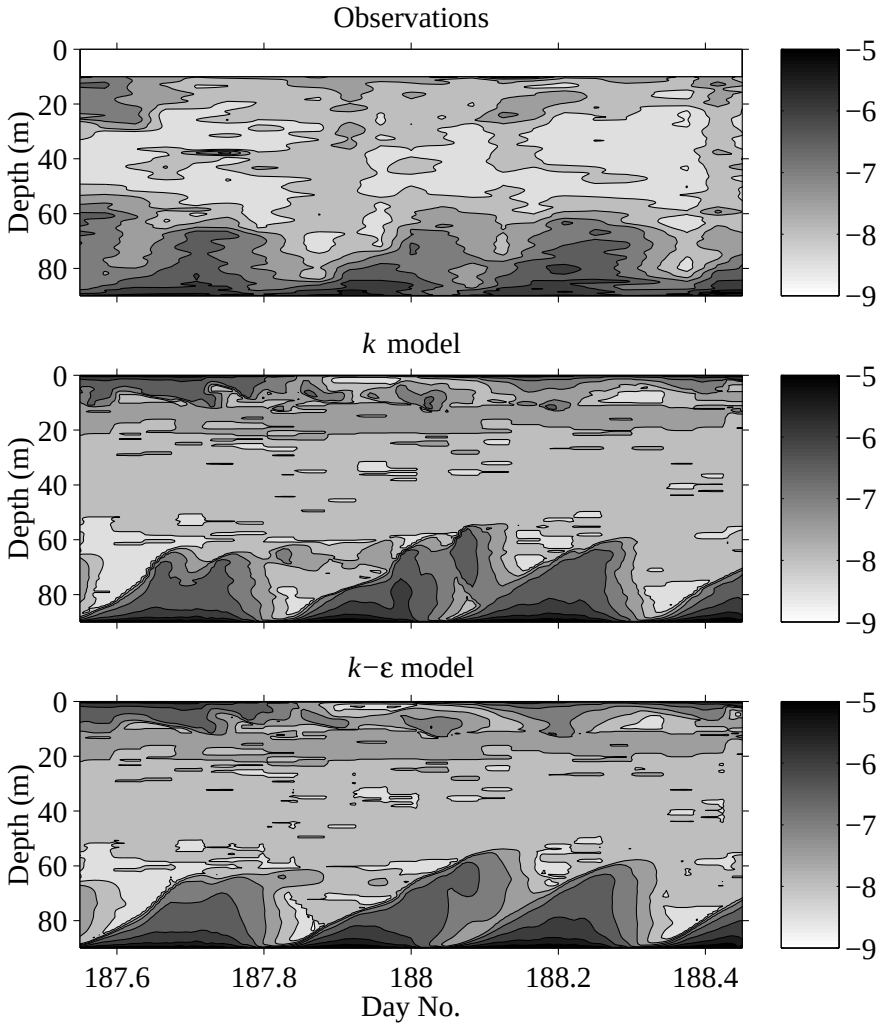

Figure 6. Isopleths of the base-10 logarithm of observed (top) and simulated dissipation ($m^2\ s^{-3}$) using the k (middle) and k-ε (bottom) models at site S1 in the Irish Sea over a 24-hour period in the summer of 1993.

boundary layer as the k model, it was necessary to increase the bottom roughness to 3 cm. These results are in contrast with those of Burchard et al. [8], where both the k-ε and the Mellor-Yamada models overestimate the height of the bottom boundary layer and the dissipation (see their Fig. 8). This is probably because Burchard et al. (i) did not consider advection and (ii) spun up their model for several tidal periods without fixing the stratification.

Finally, both the k and k-ε models overestimate the near-bottom dissipation, as can also be seen in the isopleth diagrams (Fig. 6). In-

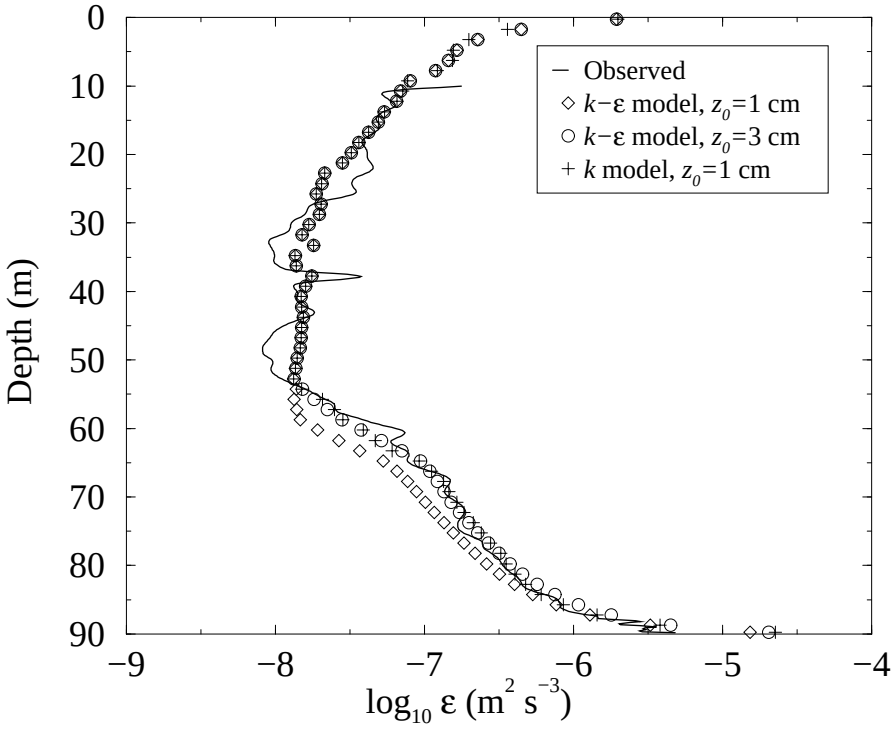

Figure 7. Mean profiles of observed and simulated dissipation at site S1 in the Irish Sea for a 24-hour period in the summer of 1993.

accuracies in the near-bed measurements [49] could perhaps contribute to this difference, a suggestion which seems plausible in view of the rather odd fluctuations in the observed mean profile near the bottom in Fig. 7.

4.6. Simulation of the mixed layer at Ocean Weather Station Papa

Finally, we will verify the proposed k model against the well-known temperature measurements at Ocean Weather Station Papa in the North Pacific at 50°N, 145°W. Like others before us [33, 26, 11] we will simulate the year 1961. As emphasized by Large et al. [29], such a verification is also a test of the forcing used. Unfortunately, the formulae for calculating the cross-surface heat and momentum fluxes are highly empirical, and there is no clear consensus on the values of the different transfer coefficients, cloud factor corrections and so on. Furthermore, when simulating oceanic data sets one may either calculate the surface fluxes in advance using observed SST (uncoupled mode) or during

the course of the simulation using the model-calculated SST (coupled mode). It may be argued that precalculating the heat fluxes makes it easier to separate merits and shortcomings of the turbulence model from those of the forcing. In this study both methods will be tested.

Solar radiation I_{rad} and its vertical extinction with depth were calculated according to Martin [33]. This implies optical type II water, 6% albedo and a cloud-cover correction given by

$$I_{rad}/I_0 = 1 - 0.756C_{cl} + 0.00357a,$$

where I_0 is the clear-sky insolation, C_{cl} is the fractional cloud cover and a is the noon solar altitude. The wind stress and the sensible and latent heat fluxes were calculated using standard bulk formulae and the transfer coefficients of Large et al. [29]. The net long-wave heat flux was also calculated using the same formula and cloud factor equation as Large et al. [29] (see Fung et al. [14]), including an enhanced emissivity of 1.0. Since the OWS Papa data set does not include salinity, the model was initialized using a climatological mean salinity profile taken from the Levitus database, to ensure that the deep halocline was correctly represented [33, 11]. The equation of state was the same as that in section 4.5 and at the lower integration boundary no-flux conditions on salt and heat were used. Simulations have been run both with and without salt fluxes through the surface caused by precipitation and evaporation, using the same mean annual cycle of precipitation as Large et al. [29]. The model was initialized with the observed temperature profile and run from March 15 to December 31. This choice of simulation period adheres to that of Large et al. [29], but we do not continue until March 15 the following year, as we will not attempt to model advective effects.

The accumulated net heat flux through the ocean surface calculated using the bulk formulae was compared to the change in total heat content of the upper 250 m from March 15 to December 31 (Fig. 8, bottom panel). To achieve reasonable agreement the solar transmission coefficient had to be increased from 0.80 [33] to 0.83. This yields an annual mean heat flux of 29 W m^{-2} for the calendar year, which is the same as that of Large et al. [29].

As in section 4.5 interior mixing is parameterized by introducing an appropriate lower limit on k. This could be used to tune the model but we will adopt the value $k_{min} = 3 \times 10^{-6}$ m^2 s^{-2} used by Burchard et al. [6].

It is clear from Fig. 9 that the qualitative agreement between models and observations is fair. However, both models overestimated the SST during the summer, the k model a little more so than the k-ε model. This is also evident from the daily mean SST plotted in Fig. 8 (top

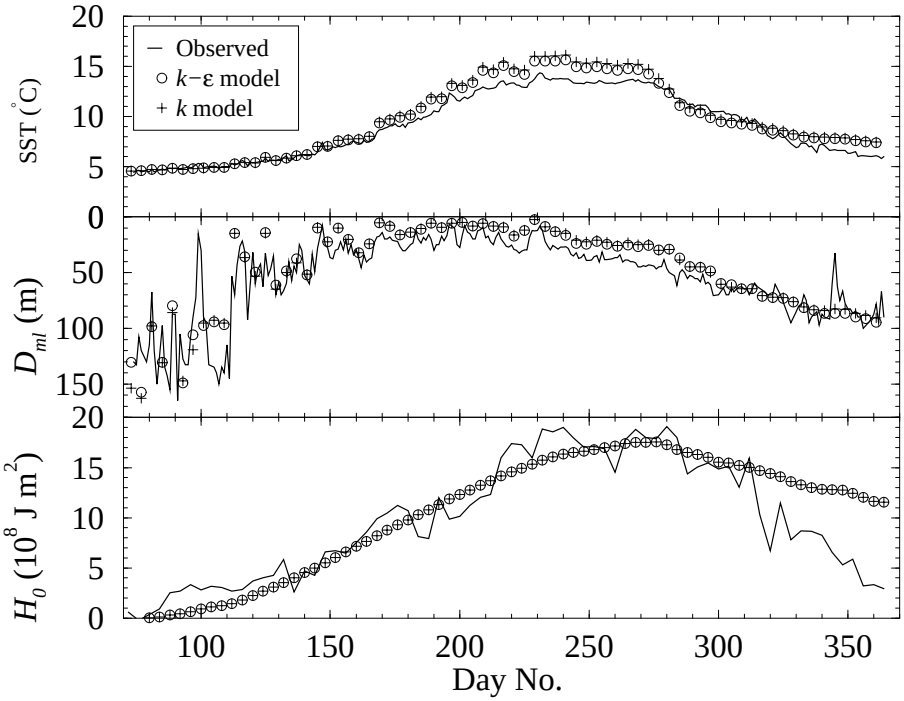

Figure 8. One-day averages of observed and modeled SST (top) and mixed layer depth (middle) in 1961. The model results are for the uncoupled mode with zero cross-surface salt flux. The bottom panel shows 4-day averages of observed and modeled heat content for the upper 250 m. The derivative of the modeled heat content is equivalent to the the net cross-surface heat flux.

panel). The main reason for this is that both models underestimated the mixed layer depth, here defined as the minimum depth at which the temperature differs from the SST by at least 0.2°C (Fig. 8, middle panel). The modeled SSTs drop sharply in early October, and both models slightly underestimated the SST by the end of October. After this the modeled SSTs level out and by the end of the year instead exceed the observations by about 1–1.5°C. This latter overestimation is probably due to horizontal winter advection of cold water, a process not accounted for in the model, as indicated by the difference between observed heat content and net accumulated cross-surface heat fluxes calculated from the bulk formulae (Fig. 8, bottom panel). See Large et al. [29] for a more extensive discussion.

In Table IV the mean monthly SST difference between model results and observations are shown for the different model configurations. As mentioned above, the k-ε model produces a slightly smaller warm bias compared to the k model. The results for both models are within the

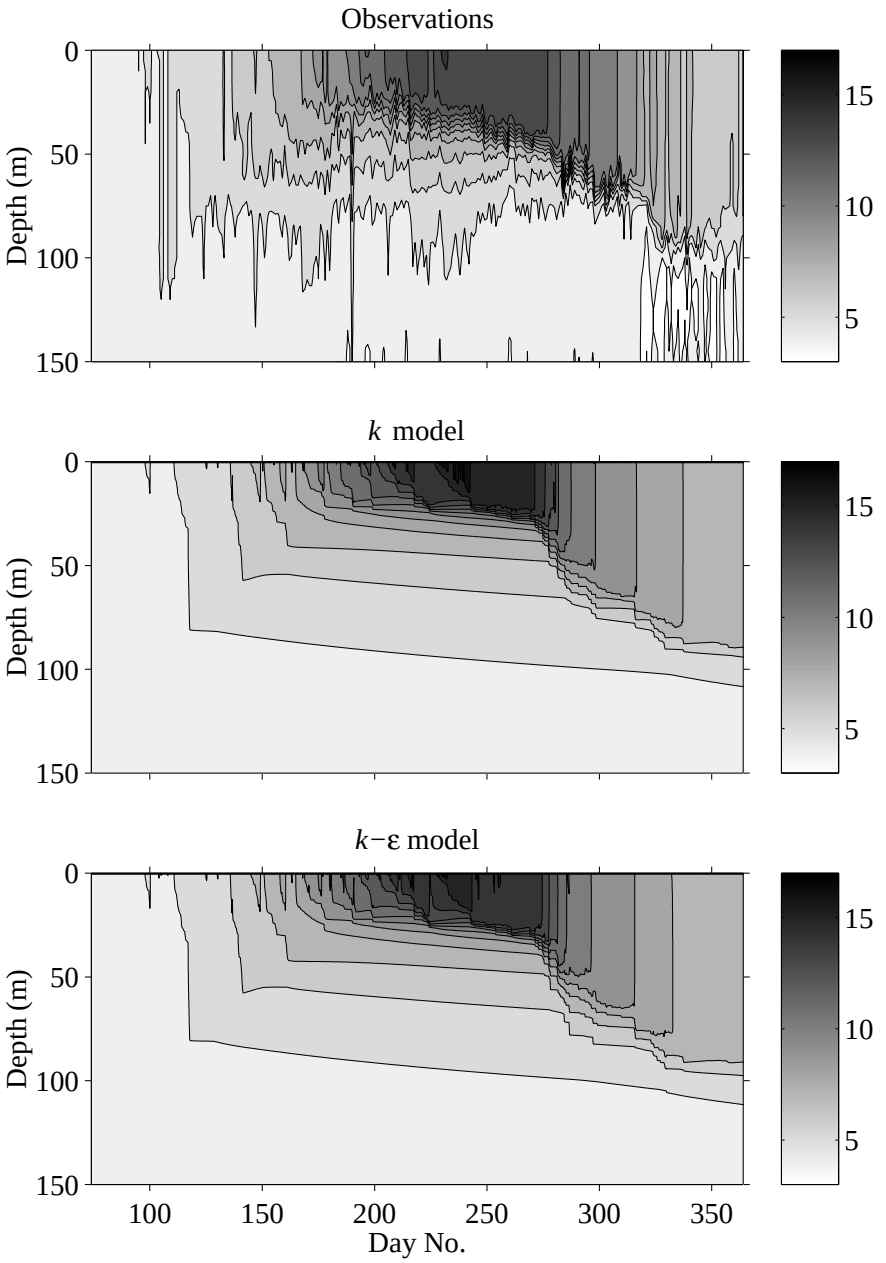

Figure 9. Isopleths of daily average temperature profiles (°C) from observations (top) and model results using the k (middle) and k-ε (bottom) models, in the upper 150 m during 1961. The model results are for the uncoupled mode with zero cross-surface salt flux. Solid contours run from 3 to 17 °C.

Table IV. Mean monthly SST difference between model results and observations for the year 1961. Negative values imply that the model underestimates the SST.

	$SST_{mod} - SST_{obs}$ (°C)								
	April	May	June	July	Aug.	Sep.	Oct.	Nov.	Dec.
k[1]	−0.30	0.07	0.56	1.13	1.94	1.88	−0.28	−0.23	1.58
k-ε[1]	−0.29	0.07	0.48	0.90	1.52	1.37	−0.61	−0.43	1.46
k[2]	−0.28	0.09	0.48	0.67	1.05	0.78	−0.90	−0.48	1.28
k-ε[2]	−0.27	0.08	0.41	0.53	0.84	0.56	−1.00	−0.53	1.29
k[3]	−0.29	0.04	0.38	0.56	0.94	0.65	−1.05	−0.62	1.20

[1] Uncoupled mode, [2] Coupled mode, [3] Coupled mode with $Q_s \neq 0$

range of those for other models presented by Large et al. [29], even though the average heat forcing used for the majority of these was only 8 W m^{-2} compared with 29 W m^{-2} in the present case.

Both models benefit partially from being run in coupled mode. The warm bias during summer is reduced, though not removed, but the underestimate of the SST during October and November increases somewhat. Finally, including a surface flux of salinity produced only a slight improvement in the mean monthly SST difference (cf. D'Alessio et al. [11]).

5. Discussion

The proposed formula for l is comparable to what some other authors have suggested. Gaspar et al. [20] use two buoyancy length scales which describe the vertical distance up or down which a fluid particle must be moved for all its turbulent energy to be converted to potential energy. These are then used to calculate two separate turbulence length scales, one for determining the eddy diffusivities and one for the dissipation. In the case of constant density gradient both reduce to $2^{1/2} l_b c_b^{-1}$, but under neutral conditions the turbulent length scales equal the distance to the nearest boundary. This implies that it is doubtful whether the model will accurately reproduce the logarithmic law.

A formula very similar to (25) is used by D'Alessio et al. [11], but with

$$\frac{1}{l_0} = \frac{1}{l_{MY}} + \frac{c_b}{l_b}$$

for locally stable conditions and $l_0 = l_{MY}$ for locally unstable conditions. Here l_{MY} is the asymptotic length scale of Mellor and Yamada [36].

Another alternative formulation for l is used by Demirov et al. [13]. In their model, l is given by a Blackadar formula in the well-mixed boundary layers with $l_0 = c\,D_{ml}$, where c is an empirical constant and D_{ml} the boundary layer thickness, but is equal to l_b elsewhere though with c_b as a function of time and depth.

The buoyancy length scale l_b has some interesting properties. Equations (23) and (19) together imply that $\varepsilon \propto kN$ when $l = l_b$. This is also true for the k-ε model in the stably stratified regime, which is readily shown by assuming stationary, homogeneous turbulence in (13) — yielding $\nu_t' \propto \varepsilon N^{-2}$ [43] — and using (19) in combination with (12). Several theories predict that $\varepsilon \propto N^p$, where $1 \leq p \leq 2$, but present-day data do not appear good enough to distinguish between them [19, 22, 18]. One reason for this may be an unknown vertical variation in k, which is not usually, nor easily, measured in the ocean.

The coefficient c_b was calibrated for a situation of stable stratification, but its value can also be estimated in an independent way. Inserting Eqs. (11) and (19) into Eq. (A10) yields

$$l^2 = \frac{\Gamma (c_\mu^0)^3}{c_\mu'} \frac{k}{N^2}, \tag{57}$$

where

$$\Gamma = \frac{R_f}{1 - R_f}. \tag{58}$$

Using (58), (A12) and (A13) it is easily shown that

$$\frac{\Gamma}{c_\mu'} = (c_\mu^0)^3 R_t,$$

which inserted into (57) implies

$$c_b = (c_\mu^0)^3 R_t^{1/2}.$$

As R_t is related to R_f through (A12), we may construct the graph in Figure 10. Reported oceanic values of R_f are often in the range $0.14 < R_f < 0.20$ [43, 25, 24], for non-patchy turbulence (cf. Arneborg [1]). It is clear from Fig. 10 that this corresponds to $0.3 < c_b < 0.5$, and that $c_b = 0.35$ corresponds to $R_f \approx 0.16$ and $\Gamma = 0.19$, values which are very close to those often used by the microstructure community (e.g Osborn [43]).

When verifying the proposed k model against oceanic data sets, we have set a minimum value on k. Since neither the k-ε nor the k model

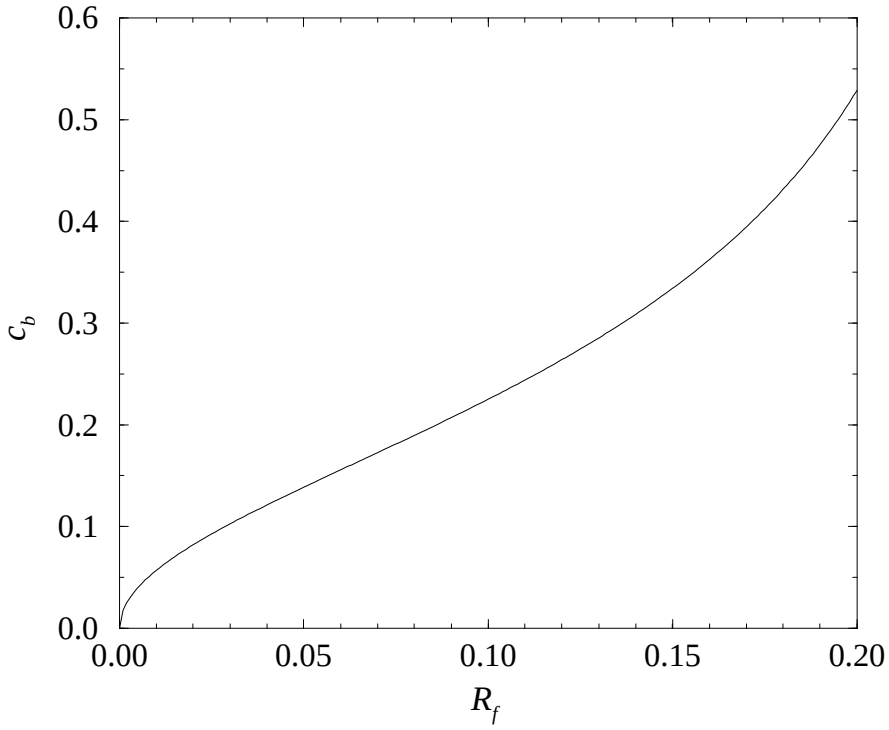

Figure 10. Dependence of c_b on the flux Richardson number R_f.

include processes such as breaking internal waves or non-resolved intermittent shear instability, some kind of interior mixing parameterization is required [29, 31]. A simple way of achieving this in TKE models is by introducing an appropriate lower limit on k. However, this only works for the k-ε model if the stratification dependent lower limit for ε given by Eq. (21) is included. To ensure a fair comparison we set $C = \left(c_\mu^0\right)^3 c_b^{-1} \approx 0.49$ (see section 2.2.2), which is about a factor two larger than the value commonly used [32]. Using (12) we see that (23) yields

$$\nu_t' \propto kN^{-1}$$

in the buoyancy-dominated regime. If we choose k_{min} with some care, we obtain

$$\nu_t' = a_0 N^{-1}$$

(cf. Gaspar et al. [20]), an expression often used to parameterize the mixing below the surface mixed layer [17, 52, 41]. The parameter a_0 is usually set to a constant value, which normally implies an increased mixing with depth. However, indirect observations in the Baltic Sea show that a_0 has a seasonal, regional as well as a vertical variation [2].

As for the parameterization of the turbulent length scale during convection, it is not evident that c_b should have the same value as in the case of stable stratification. However, as the convection experiments were so well simulated we saw no reason to assign another value of c_b for the convective case. Further, it should be remembered that the large coherent structures important in convection are not well described by the small-scale, isotropic turbulence which is the fundamental assumption in TKE closure models. As discussed in section 4.4, the k-ε and the Mellor-Yamada models both employ the eddy diffusivity concept which only allows down-gradient transport, hence neglecting nonlocal effects. Kantha and Clayson [26] as well as D'Alessio et al. [11] have extended the TKE closure approach by adding nonlocal and counter-gradient contributions. Even so, the basic assumption is that the instantaneous flow properties can be decomposed into mean components and turbulent fluctuations. This is hardly valid for the case of free convection in a model which is one-dimensional in the vertical. Still, as stated above, TKE models yield reasonable estimates for the resulting mixing. The reason for this is probably that the total energy available for mixing is reasonably well budgeted by the equation for the TKE, which is then converted to potential energy via mixing. For a more detailed discussion of modeling convection, see the review by Large et al. [29].

The tendency to produce a too shallow mixed layer and too high SST during a stabilizing surface buoyancy flux (see section 4.6) is a general problem of most TKE closure models [33, 35, 29, 6]. The second-moment closure of D'Alessio et al. [11] appears to resolve this, but it is unclear exactly what heat forcing has been used by these authors. Furthermore, this more advanced model produces too high summer temperatures even when the vertical resolution was increased to 2.5 m [11]. Note that in our simulations we have used $\Delta z = 0.5$ m (see Table B1). The results of Kantha and Clayson [26] and Burchard et al. [6] emphasize the importance of the interior mixing parameterization. In this context it should be mentioned that the observations indicate a much sharper thermocline in September–October than that produced by the two models in the present study, which could be associated with deep water advection (Fig. 9).

The adjustment of the coefficients in the stability functions of Launder [30] clearly produce very good agreement with the empirical Monin-Obukhov similarity functions of Högström [23] [Eqs. (46)–(47)]. However, this also reduces the eddy diffusivities in the case of a stabilizing buoyancy flux, which in turn aggravates the problems of insufficient mixed layer depth and too high SST. It is not evident that the oceanic surface layer behaves in the same way as the atmospheric surface layer, from which the data determining the similarity functions originate.

The surface layer of the atmosphere is approximately equivalent to the upper few meters in the ocean, a region where surface waves and Langmuir-type motions may be as important for turbulence as vertical shear. Hence, for practical purposes it is questionable whether the performance of ocean mixed-layer models based on TKE closure should be expected to agree with the empirical Monin-Obukhov functions.

Finally, it would be straightforward to extend the model in the manner of Kantha and Clayson [26] and D'Alessio et al. [11] to include counter-gradient and non-local fluxes. Alternative interior mixing parameterizations, such as those of Large et al. [29] and Liungman [31], could also easily be added.

6. Conclusions

The conclusions of the paper may be summarized as follows:

- For geophysical applications such as the ones tested here, the performance of the presented one-equation k model is just as good as the that of the more sophisticated two-equation k-ε model. As the code of the one-equation model is slightly faster than that of two-equation models, the proposed k model may be an alternative for CPU demanding simulations such as in climate prediction.
- The proposed stability functions agree rather well with the recent empirical formulas of Högström [23]. In contrast, previously published stability functions predict a near-neutral Prandtl number σ_t^0 much lower than unity, whereas observations suggest $\sigma_t^0 = 1.0$ [59, 23]. Further, most other published stability functions predict too low Prandtl numbers in stable stratification, also in disagreement with recent data.

Acknowledgements

Lars Axell gratefully acknowledges the financial support of the European Commission, contract MAS3-CT96-0058 (DG 12-D), and the Swedish Meteorological and Hydrological Institute. Both authors thank Anders Omstedt, Hans Burchard, and anonymous reviewers for valuable comments on an earlier draft. We also thank Tom Rippeth for providing the Irish Sea data [the collection of the data was funded by NERC grant GR3/7009 and made available through the EU Concerted Action CARTUM (PL97 15 11)] and Paul Martin for providing the OWS Papa data.

Appendix A: Estimating the coefficients in the stability functions

Assuming local equilibrium (that is, assuming steady state and neglecting transport terms), Launder [30] derived the stability functions α, β and γ, related to c_μ and c'_μ through

$$c_\mu = \frac{\alpha\beta}{(c_\mu^0)^3} \tag{A1}$$

and

$$c'_\mu = \frac{\alpha\gamma}{(c_\mu^0)^3}. \tag{A2}$$

Here, $\alpha = \overline{w'^2}/k$ is the non-dimensional vertical normal-stress component, which is stability dependent, and β and γ are further stability corrections. Launder argues that they should have the following functional forms:

$$\alpha = \frac{2}{3}(1-\phi) - 2\phi\frac{R_f}{1-R_f}, \tag{A3}$$

$$\beta = \frac{\phi - \phi\phi'_T\gamma R_t}{1 + \phi\phi_T R_t}, \tag{A4}$$

$$\gamma = \frac{\phi_T}{1 + \phi'_T c'_T R_t}, \tag{A5}$$

where R_f is the flux Richardson number (see definition below) and R_t is the turbulent Richardson number defined in (29).

During neutral conditions, $N^2 = 0$, and hence $R_f = 0$ and $R_t = 0$. From (A3)–(A5) we see that this implies that the neutral values of α, β and γ are $\alpha_0 = \alpha(0) = \frac{2}{3}(1-\phi)$, $\beta_0 = \beta(0) = \phi$ and $\gamma_0 = \gamma(0) = \phi_T$, respectively. The corresponding neutral values of the stability functions then become

$$c_\mu(0) = \frac{\alpha_0\beta_0}{(c_\mu^0)^3} = \frac{\frac{2}{3}(1-\phi)\phi}{(c_\mu^0)^3}, \tag{A6}$$

$$c'_\mu(0) = \frac{\alpha_0\gamma_0}{(c_\mu^0)^3} = \frac{\frac{2}{3}(1-\phi)\phi_T}{(c_\mu^0)^3}. \tag{A7}$$

Following Burchard et al. [8], we have $c_\mu(0) = c_\mu^0 = 0.5562$. Solving for ϕ in Eq. (A6) yields $\phi = \frac{1}{2} \pm 0.326$. Choosing the lower value, which is closest to Launder's estimate, we have

$$\phi = 0.174.$$

According to Högström [23] the turbulent Prandtl number approaches 1.0 when the stratification approaches neutral conditions, that is $c_\mu(0) = c'_\mu(0)$. Equations (A6) and (A7) then require $\phi_T = \phi$, that is,

$$\phi_T = 0.174.$$

The value of the coefficient ϕ'_T can be calculated from the ratio $\overline{u'T'}/\overline{w'T'}$ evaluated for non-buoyant conditions,

$$\frac{\overline{u'T'}}{\overline{w'T'}} = \frac{\overline{u'w'}}{\overline{w'^2}}\left(1 + \frac{\phi'_T}{\phi}\right) \tag{A8}$$

[30, 53]. Here the primes denote turbulent quantities, and

$$\frac{\overline{u'w'}}{\overline{w'^2}} = \frac{\sqrt{\frac{2}{3}(1-\phi)\phi}}{\frac{2}{3}(1-\phi)}.$$

According to the data of Webster [58], the fraction $\overline{u'T'}/\overline{w'T'}$ in (A8) is close to unity (the exact value is adopted). Solving for ϕ'_T in (A8) and using the new value of ϕ yields

$$\phi'_T = 0.136.$$

Finally, the coefficient c'_T was estimated by Launder from the decay of temperature fluctuations in grid turbulence, and as its value does not depend on ϕ, ϕ_T, or ϕ'_T [53] we adopt Launder's value and set

$$c'_T = 1.6.$$

To be able to calculate the stability functions c_μ and c'_μ using (A1)–(A2) an expression for the flux Richardson number R_f, which may be written as

$$R_f = -\frac{P_b}{P_s} = \frac{\nu'_t N^2}{\nu_t\left[\left(\frac{\partial u}{\partial z}\right)^2 + \left(\frac{\partial v}{\partial z}\right)^2\right]}, \tag{A9}$$

is required in (A3). Here (14) and (15) have been used. However, (A9) is not very useful in ocean models as they are unable to resolve the small-scale shear, possibly due to unresolved internal waves, below the surface mixed layer. To find an alternative formulation for R_f, let us consider the local-equilibrium form of the TKE equation (13), that is $P_s + P_b = \varepsilon$. Using (14), (15) and (A9) we then obtain the so-called Osborn formula:

$$\nu'_t = \frac{R_f}{1 - R_f}\frac{\varepsilon}{N^2} \tag{A10}$$

(cf. Osborn [43]). Now, inserting (12), (19), (32) and (29) into (A10) yields

$$\alpha\gamma R_t = \frac{R_f}{1-R_f}, \tag{A11}$$

or

$$\left[\frac{2}{3}(1-\phi) - 2\phi\frac{R_f}{1-R_f}\right]\frac{\phi_T R_t}{1+\phi_T' c_T' R_t} = \frac{R_f}{1-R_f}.$$

Solving for $R_f/(1-R_f)$ we arrive at

$$\frac{R_f}{1-R_f} = \frac{c_1 R_t}{1+c_2 R_t}, \tag{A12}$$

where

$$c_1 = \frac{2}{3}(1-\phi)\phi_T = (c_\mu^0)^4 \approx 0.0957,$$

$$c_2 = \phi_T' c_T' + 2\phi\phi_T \approx 0.277.$$

Now, using (A12) in (A11) we see that $\alpha\gamma = c_1/(1+c_2 R_t)$, or

$$\begin{aligned} c_\mu' &= \frac{c_\mu^0}{1+c_2 R_t} \\ &\approx \frac{0.556}{1+0.277 R_t}. \end{aligned} \tag{A13}$$

Equations (30), (A1) and (A2) imply that the turbulent Prandtl number is equal to $\sigma_t = \beta/\gamma$, which after some algebra may be written as

$$\begin{aligned} \sigma_t &= \frac{\phi/\phi_T + (c_T'/\phi_T - 1)\phi\phi_T' R_t}{1+\phi\phi_T R_t} \\ &\approx \frac{1+0.193 R_t}{1+0.0302 R_t}. \end{aligned} \tag{A14}$$

Since $c_\mu = c_\mu' \sigma_t$ [Eq. (30)], we have

$$\begin{aligned} c_\mu &= \frac{c_\mu^0[\phi/\phi_T + (c_T'/\phi_T - 1)\phi\phi_T' R_t]}{(1+c_2 R_t)(1+\phi\phi_T R_t)} \\ &\approx \frac{0.556 + 0.108 R_t}{1+0.308 R_t + 0.00837 R_t^2}. \end{aligned} \tag{A15}$$

Equations (A13)–(A15) are identical with (31)–(33) in section 2.2.3.

Table B1. Numerical parameters used in the simulations.

Simulation	Δt (s)	Δz (m)	z_0 (cm)	D (m)
Price [44]	30	0.25	1	50
Entrainment experiments	60	0.5	1	200
Deardorff et al. [12]	0.5	0.005	0	0.355
Irish Sea	30	0.5	1 (3)	90
OWS Papa	120	1	0	250

Appendix B: Numerical implementation

The k model was implemented in the one-dimensional equation solver PROBE [53, 54]. This flexible software has been used extensively for simulating various fluid dynamical and geophysical situations, both in the atmosphere, the ocean and in lakes [55, 39, 42]. The k-ε model is a built-in feature of PROBE, which can also handle a varying hypsography, advective in- and outflows and various formulations of the stability functions. The discretization does not employ a so-called staggered grid. Instead, all variables are co-located at the center of the grid cells, which need not be equidistant.

In the standard setup constant minimum values for k, ε and ν_t have been used: 10^{-10} m^2 s^{-2} for k, 10^{-10} m^2 s^{-3} for ε, and the laminar viscosity $\nu = 1.3 \times 10^{-6}$ m^2 s^{-1} for ν_t. Should ν_t fall below this value then ν_{eff} is set to the value of ν and ν'_{eff} is set to the corresponding laminar diffusivities for salt and heat, respectively.

In Table B1 the time step Δt, the vertical resolution Δz, the bottom roughness z_0 and the total depth D used in the various simulations are summarized. If z_0 is given as 0, then a smooth-wall boundary condition has been used.

References

1. Arneborg, L.: 2000, 'Oceanographic studies of internal waves and diapycnal mixing'. Ph.D. thesis, Dept. of Oceanography, Earth Sciences Centre, Göteborg University, Box 460, SE–405 30 Göteborg, Sweden.
2. Axell, L. B.: 1998, 'On the variability of Baltic Sea deepwater mixing'. *J. Geophys. Res.* **103**, 21667–21682.
3. Blackadar, A. K.: 1962, 'The vertical distribution of wind and turbulence exchange in a neutral atmosphere'. *J. Geophys. Res.* **67**, 3095–3102.

4. Blanke, B. and P. Delecluse: 1993, 'Variability of the tropical Atlantic Ocean simulated by a General Circulation Model with two different mixed-layer physics'. *J. Phys. Oceanogr.* **23**, 1363–1388.
5. Burchard, H. and H. Baumert: 1995, 'On the performance of a mixed-layer model based on the k-ε turbulence closure'. *J. Geophys. Res.* **100**, 8523–8540.
6. Burchard, H., K. Bolding, and M. Villarreal: 1999, 'GOTM, a general ocean turbulence model. Theory, implementation and test cases'. Technical report, European Commission, Report EUR 18745, 103 pp.
7. Burchard, H. and O. Petersen: 1999, 'Models of turbulence in the marine environment — A comparative study of two-equation turbulence models'. *J. Mar. Sys.* **21**, 29–53.
8. Burchard, H., O. Petersen, and T. Rippeth: 1998, 'Comparing the performance of the Mellor-Yamada and the k-ε two-equation turbulence models'. *J. Geophys. Res.* **103**, 10543–10554.
9. Businger, J., J. Wyngaard, Y. Izumi, and E. Bradley: 1971, 'Flux-profile relationships in the atmospheric surface layer'. *J. Atmos. Sci.* **28**, 181–189.
10. Champagne, F. H., V. G. Harris, and S. Corrsin: 1970, 'Experiments on nearly homogeneous shear flow'. *J. Fluid Mech.* **41**, 81–139.
11. D'Alessio, S. J. D., K. Abdella, and N. A. McFarlane: 1998, 'A new second-order turbulence closure scheme for modeling the oceanic mixed layer'. *J. Phys. Oceanogr.* **28**, 1624–1641.
12. Deardorff, J. W., G. E. Willis, and D. Lilly: 1969, 'Laboratory investigation of non-steady penetrative convection'. *J. Fluid Mech.* **35**, 7–31.
13. Demirov, E., W. Eifler, M. Ouberdous, and N. Hibma: 1998, 'ISPRAMIX—a three-dimensional free surface model for coastal ocean simulations and satellite data assimilation on parallel computers'. Technical Report EUR 18129EN, European Commission, 76 pp.
14. Fung, I. Y., D. E. Harrison, and A. A. Lacis: 1984, 'On the variability of the net longwave radiation at the ocean surface'. *Rev. Geophys.* **22**, 177–193.
15. Galperin, B., L. H. Kantha, S. Hassid, and A. Rosati: 1988, 'A quasi-equilibrium turbulent energy model for geophysical flows'. *J. Atmos. Sci.* **45**, 55–62.
16. Galperin, B., A. Rosati, L. H. Kantha, and G. L. Mellor: 1989, 'Modeling rotating stratified turbulent flows with application to oceanic mixed layers'. *J. Phys. Oceanogr.* **18**, 901–916.
17. Gargett, A. E.: 1984, 'Vertical eddy diffusivity in the ocean interior'. *J. Mar. Res.* **42**, 359–393.
18. Gargett, A. E.: 1990, 'Do we really know how to scale the turbulent kinetic energy dissipation rate ε due to breaking of oceanic internal waves?'. *J. Geophys. Res.* **95**, 15971–15974.
19. Gargett, A. E. and G. Holloway: 1984, 'Dissipation and diffusion by internal wave breaking'. *J. Mar. Res.* **42**, 15–27.
20. Gaspar, P., Y. Grégoris, and J.-M. Lefevre: 1990, 'A simple eddy kinetic energy model for simulations of the vertical mixing: tests at station Papa and Long-Term Upper Ocean Study site'. *J. Geophys. Res.* **95**, 16179–16193.
21. Goosse, H., E. Deleersnijder, and T. Fichefet: 1999, 'Sensitivity of a global coupled ocean-sea ice model to the parameterization of vertical mixing'. *J. Geophys. Res.* **104**, 13681–13695.
22. Gregg, M. C.: 1989, 'Scaling turbulent dissipation in the thermocline'. *J. Geophys. Res.* **94**, 9686–9698.

23. Högström, U.: 1996, 'Review of some basic characteristics of the atmospheric surface layer'. *Boundary-Layer Meteorol.* **78**, 215–246.
24. Itsweire, E., J. Koseff, D. Briggs, and J. Ferziger: 1993, 'Turbulence in stratified shear flows: Implications for interpreting shear-induced mixing in the ocean'. *J. Phys. Oceanogr.* **23**, 1508–1522.
25. Ivey, G. and J. Imberger: 1991, 'On the nature of turbulence in a stratified fluid. Part I: The energetics of mixing'. *J. Phys. Oceanogr.* **21**, 650–658.
26. Kantha, L. H. and A. C. Clayson: 1994, 'An improved mixed layer model for geophysical applications'. *J. Geophys. Res.* **99**, 25235–25266.
27. Kato, H. and O. Phillips: 1969, 'On the penetration of a turbulent layer into a stratified fluid'. *J. Fluid Mech.* **37**, 643–655.
28. Kundu, P. K.: 1990, 'Fluid mechanics'. Academic Press, Inc., 638 pp.
29. Large, W. G., J. C. McWilliams, and S. C. Doney: 1994, 'Oceanic vertical mixing: A review and a model with a nonlocal boundary layer parameterization'. *Rev. Geophys.* **32**, 363–403.
30. Launder, B. E.: 1975, 'On the effects of a gravitational field on the turbulent transport of heat and momentum'. *J. Fluid Mech.* **67**, 569–581.
31. Liungman, O.: 2000, 'Tidally forced internal wave mixing in a k-ε model framework applied to fjord basins'. *J. Phys. Oceanogr.* **30**, 352–368.
32. Luyten, P. J., E. Deleersnijder, J. Ozer, and K. G. Ruddick: 1996, 'Presentation of a family of turbulence closure models for stratified shallow water flows and preliminary application to the Rhine outflow region'. *Cont. Shelf Res.* **16**, 101–130.
33. Martin, P. J.: 1985, 'Simulation of the mixed layer at OWS November and Papa with several models'. *J. Geophys. Res.* **90**, 903–916.
34. McPhee, M. G.: 1994, 'On the turbulent mixing length in the oceanic boundary layer'. *J. Phys. Oceanogr.* **24**, 2014–2031.
35. Mellor, G. L.: 1989, 'Retrospect on oceanic boundary layer modeling and second moment closure'. In: *Proc. Fifth Aha Huliko'a Hawaiian Winter Workshop.* Honolulu, HI, Hawaii Institute of Geophysics, 251–272.
36. Mellor, G. L. and T. Yamada: 1974, 'A hierarchy of turbulence closure models for planetary boundary layers'. *J. Atmos. Sci.* **31**, 1791–1806.
37. Mellor, G. L. and T. Yamada: 1982, 'Development of a turbulence closure model for geophysical problems'. *Rev. Geophys.* **20**, 851–875.
38. Moum, J., D. Caldwell, and C. Paulson: 1989, 'Mixing in the equatorial surface layer and thermocline'. *J. Geophys. Res.* **94**, 2005–2021.
39. Nordblom, O.: 1997, 'Numerical simulation of the atmospheric surface layer'. Master's thesis, Department of Environmental Engineering, Division of Water Resources Engineering, Luleå University of Technology, Sweden.
40. Oakey, N.: 1982, 'Determination of the rate of dissipation of turbulent energy from simultaneous temperature and velocity shear microstructure measurements'. *J. Phys. Oceanogr.* **12**, 256–271.
41. Omstedt, A.: 1990, 'Modelling the Baltic Sea as thirteen sub-basins with vertical resolution'. *Tellus* **42A**, 286–301.
42. Omstedt, A. and L. B. Axell: 1998, 'Modeling the seasonal, interannual, and long-term variations of salinity and temperature in the Baltic proper'. *Tellus* **50A**, 637–652.
43. Osborn, T. R.: 1980, 'Estimates of the local rate of vertical diffusion from dissipation measurements'. *J. Phys. Oceanogr.* **10**, 83–89.
44. Price, J. F.: 1979, 'On the scaling of stress-driven entrainment experiments'. *J. Fluid Mech.* **90**, 509–529.

45. Rodi, W.: 1980, 'Turbulence models and their application in hydraulics—A state-of-the-art review'. International Association for Hydraulic Research, Rotterdamseweg 185, P.O. Box 177, 2600 MH Delft, The Netherlands.
46. Rodi, W.: 1987, 'Examples of calculation methods for flow and mixing in stratified flows'. *J. Geophys. Res.* **92**, 5305–5328.
47. Rosati, A. and K. Miyakoda: 1988, 'A General Circulation Model for upper ocean simulation'. *J. Phys. Oceanogr.* **18**, 1601–1626.
48. Simpson, J. H. and D. G. Bowers: 1984, 'The role of tidal stirring in controlling the seasonal heat cycle in shelf seas'. *Annales Geophysicae* **2**, 411–416.
49. Simpson, J. H., W. R. Crawford, T. P. Rippeth, A. R. Campbell, and J. V. S. Cheok: 1996, 'The vertical structure of turbulent dissipation in shelf seas'. *J. Phys. Oceanogr.* **26**, 1579–1590.
50. Skyllingstad, E. D., W. D. Smyth, J. N. Moum, and H. Wijesekera: 1999, 'Upper-ocean turbulence during a westerly wind burst: a comparison of large-eddy simulation results and microstructure measurements'. *J. Phys. Oceanogr.* **29**, 5–28.
51. Squires, K. D. and H. Yamazaki: 1995, 'Preferential concentration of marine particles in isotropic turbulence'. *Deep Sea Res.* **42**, 1989–2004.
52. Stigebrandt, A.: 1987, 'A model for the vertical circulation of the Baltic deep water'. *J. Phys. Oceanogr.* **17**, 1772–1785.
53. Svensson, U.: 1978, 'A mathematical model for the seasonal thermocline'. Report No. 1002, Dept. of Water Res. Eng., Lund Inst. of Technology, Lund, Sweden.
54. Svensson, U.: 1998, 'PROBE. Program for boundary layers in the environment. System description and manual'. Report Oceanography No. 24, Swedish Meteorological and Hydrological Institute, SE–601 76 Norrköping, Sweden.
55. Svensson, U. and J. Sahlberg: 1989, 'Formulae for pressure gradients in one-dimensional lake models'. *J. Geophys. Res.* **94**, 4939–4946.
56. Tennekes, H. and J. L. Lumley: 1972, 'A first course in turbulence'. The MIT Press, 300 pp.
57. Turner, J. S.: 1973, 'Buoyancy Effects in Fluids'. Cambridge Univ. Press, London and New York, 367 pp.
58. Webster, C. A. G.: 1964, 'An experimental study of turbulence in a density stratified shear flow'. *J. Fluid Mech.* **19**, 221–245.
59. Wieringa, J.: 1980, 'A reevaluation of the Kansas mast influence on measurements of stress and cup anemometer overspeeding'. *Boundary-Layer Meteorol.* **18**, 411–430.
60. Xing, J. and A. M. Davies: 1995, 'Application of three dimensional turbulence energy models to the determination of tidal mixing and currents in a shallow sea'. *Prog. Oceanogr.* **35**, 153–205.

Address for Offprints:
Lars Axell,
Swedish Meteorological and Hydrological Institute,
SE–601 76 Norrköping, Sweden
e-mail: Lars.Axell@smhi.se
Fax: +46 11 495 80 01